A Nano-Mechanical Resonator with 10nm Hafnium-Zirconium Oxide Ferroelectric Transducer

M. Ghatge, G. Walters, T. Nishida and R. Tabrizian
Department of Electrical and Computer Engineering, University of Florida, Gainesville, FL, USA
email: ruyam@ufl.edu

***Abstract*—**This paper reports, for the first time, on a 10nm hafnium-zirconium oxide ($Hf_{0.5}Zr_{0.5}O_2$) (HZO) piezoelectric transducer for nano-electromechanical systems (NEMS). The super-thin HZO films are engineered through atomic-level stacking, capping with titanium nitride (TiN) electrodes, and proper thermo-mechanical treatment, to realize ferroelectric transducers with large piezoelectric properties. The developed 10nm transducer is used for excitation of a silicon-based multi-morph nano-mechanical resonator, with an overall thickness of ~350nm, at ~4MHz. The developed resonator, along with 120nm aluminum-nitride (AlN) transduced counterparts, are also used as test-vehicles to characterize ferroelectric and piezoelectric properties. Benefiting from large piezoelectric coefficient ($e_{31,HZO} \approx 2.3e_{31,AlN}$), fully conformal deposition, and CMOS-compatibility, ALD-deposited 10nm HZO transducer paves the way for realization of truly monolithic cm- and mm-wave RF front-ends for the emerging 5G wireless communication systems, and extreme / 3D integration of NEMS sensors and actuators.

I. Introduction

Ever since the advent of micro- and nano-electro-mechanical resonators, the need for large electromechanical coupling coefficient, extreme frequency scalability, and CMOS processing compatibility have been the governing drivers for the advancement of thin-film piezoelectric transducers. The development of high quality piezoelectric films realized high-performance bulk acoustic resonators and filters, and enabled RF front-end modules for wireless mobile systems.

However, the forthcoming 5G era, with ambitious target of the extension of wireless communication to mm-wave regime, has raised an unprecedented urgency for transformation of piezoelectric films and acoustic resonator architectures. To fulfill the demand for extreme frequency scaling to mm-wave regime, the quest for material and architectural transformation of the acoustic resonator technology continues. While the development of fin-based resonator architectures [1, 2] and the use of single crystal films and substrates help further the scaling limits beyond the current state, the ultimate bound of the frequency scaling is set by the technological limitations in piezoelectric film thickness minuaturization. With the frequency of bulk acoustic resonators inversely proportional to the thickness of the piezoelectric film, extreme frequency scaling to mm-wave regime requires radical thickness miniaturization to sub-100nm. Such a miniaturization is substantially inhibited by the nucleation, crystallization, and texture development processes in current piezoelectric film deposition techniques (e.g. magnetron-sputtering and MOCVD), and drastically degrade the electromechanical coupling and energy dissipation coefficients [3].

To address this technological gap, the paper demonstrates, for the first time, the use of piezoelectric properties of a 10nm atomically engineered ferroelectric hafnium-zirconium oxide (HZO) film for transduction of nano-mechanical resonators. Though HZO is widely studied for FeFET and FeRAM devices [4], it has not yet been applied in piezoelectric transducers. Three unique characteristics of ferroelectric HZO stand out in comparison with other ferroelectric materials that are profoundly transformative for advanced devices: CMOS compatibility, occurrence of ferroelectricity, and hence piezoelectricity, in sub-10nm films, and the capability to engineer the ferroelectric properties through atomic layering of mono-layers of dopants [5]. Furthermore, the extreme thickness scaling makes it a promising candidate for nano-acoustic resonators in the mm-wave regime. Finally, the conformal nature of ALD enables its 3D integration for the realization of fin-based resonators, and sidewall transducers for very-large-scale-integrated sensors and actuator arrays.

II. Atomically Engineered HZO Film

ALD deposited HZO films are typically amorphous due to the low thermal budget operation but can be engineered into crystallinity with rapid thermal annealing (RTA). The non-centrosymmetric orthorhombic crystal phase achieved after RTA exhibits a ferroelectric behavior. A capping layer, such as titanium nitride (TiN), helps suppress the monoclinic phase and promotes the orthorhombic phase during the RTA process [6, 7]. Doped HfO_2 have been explored extensively for ferroelectricity, however the choice of 1:1 binary HfO_2:ZrO_2 is driven by its low annealing temperature and high polarization [8]. The substrate or bottom electrode on which HZO is grown has been shown to have a pronounced effect on its ferroelectric response and thus piezoelectricity. The films grown on top of (002) c-axis oriented AlN and subsequently sputtered Mo are observed to show a higher polarization than films grown on Ge or TiN/Si as substrate or bottom electrode. The ferroelectric nature of HZO can be further exploited to tune the material properties with an applied DC voltage or to permanently reorient the spontaneous polarization. Unlike PZT, an order of magnitude higher coercive field strength of HZO increases its resilience to internal depolarization or signal fluctuations thus widening its material tuning capability for piezoelectricity [6]. The high-*k* dielectric nature of HZO along with its

piezoelectricity can be used for dual electrostatic/piezoelectric hybrid-actuation for low-voltage operation.

III. Multi-morph Resonator Design

A multi-morph nano-mechanical resonator is used for characterization of HZO piezoelectric properties. The resonator is formed by stacking HZO/TiN, c-axis oriented AlN/Mo, and Si. Benefiting from two independent piezoelectric transduction ports (i.e. HZO and AlN), various drive/sense mechanisms are used. Two-port resonators with asymmetric transducer designs (port-1 AlN, port-2 HZO) are used (Fig. 1(a)) to evaluate the frequency response for HZO-actuate/AlN-sense driving mechanism. To aviod the potential interference of AlN, alternative architecture with HZO-only transducer is also studied (Fig. 1(b)). Fig. 2 details the resonator stack through the high-resolution cross-sectional TEM (HR-XTEM) image.

IV. Fabrication Process

Fig. 3 summarizes the fabrication process used for implementation of the multi-morph nano-mechanical resonator. AlN film (120nm) sandwiched between top and bottom 50nm molybdenum (Mo) layers are magnetron-sputtered on top of a 70nm device layer SOI substrate. Top Mo is patterned to serve as the ground (GND) for the HZO transduction port. An ALD 10nm-HZO / 10nm-TiN stack is then deposited using alternating series of pulses: tetrakis (dimethylamino) zirconium (IV), followed by a water (H_2O) to oxidize the layer and tetrakis (dimethylamido) hafnium (IV), again followed by H_2O for oxidation. By alternating equal cycles of HfO_2 and ZrO_2 a 1:1 binary of 10nm HZO is achieved. This is followed by tetrakis (dimethylamido) titanium (IV) and nitrogen plasma cycles to deposit the 10nm TiN. The TiN capping layer is selectively patterned for the HZO transduction regions using a Cl_2/H_2 based plasma process. HZO is then etched using BOE to get access to AlN in all regions except the HZO transducer area. Following HZO/TiN selective etching, RTA at 500^0C for 20 seconds is used to crystalize the HZO in its ferroelectric phase. The crystalline form of the HZO film is evident from the diffraction pattern shown in TEM image (Fig. 2(b)). 30nm platinum (Pt) $RF_{in/out}$ electrodes are sputtered and patterned using a liftoff process. Bottom Mo (serving as GND for the AlN transducer) is accessed by dry etch of the 120nm AlN outside the device area. The lateral geometry of the device is then defined with selective etching of the 120nm AlN / 50nm Mo / 70nm Si in a RIE/ICP process. Finally, the devices are released from the top side by etching the buried oxide layer through the trench and etch holes using HF acid.

V. Characterization Results

Various electrical and optical characterization schemes are used to evaluate the performance of the resonator and the ferroelectric and piezoelectric properties of HZO (Fig. 4). Fig. 5 shows the two-port frequency response of the device in Fig. 1(a), highlighting the resonance peak with a Q_{max} of ~50 (in air) at ~4MHz. Beside two-port electrical characterization, the HZO-only transduced resonator (Fig. 1(b)) is optically characterized by monitoring the out-of-plane vibration amplitude using a digital holographic microscope (DHM) and the results are compared with AlN-only transduced counterpart (Fig. 6). Such a comparison enables characterization of piezoelectric coefficient of HZO, resulting in $e_{31,HZO} \approx 2.3e_{31,AlN}$. Fig. 7 (a,b) show the short-span frequency response of the resonator in Fig. 1(a) for various excitation voltages applied to HZO- and AlN-transduction ports, respectively, highlighting the transition to nonlinear operation regime. Fig. 8 compares the improved P-V response of 10nm HZO on top of AlN/Mo with typical TiN/Si electrodes. Fig. 9 shows the P-V response of the HZO on top of the resonator after the device release using HF. The reduced polarization (P_r) compared to Fig. 8 is attributed to the effect of HF etch on HZO through the the trench and etch holes and the smaller ferroelectric capacitor area on resonator. The P-V response can be improved through exploiting backside dry-release and increasing the transduction area. Fig. 10 shows the permittivity response of HZO demonstrating tunable high-*k* properties.

VI. Conclusion and Discussion

This paper demonstrates the thinnest ever-reported CMOS-compatible piezoelectric transducer using 10nm ferroelectric HZO film. Atomically deposited ferroelectric HZO films are engineered to demonstrate large piezoelectric properties, and used for excitation of multi-morph nano-mechanical resonator. Various schemes, including isolated HZO- and AlN-transduction ports, along with different electrial and optical characterization are used to extract the ferroelectric and piezoelectric properties of HZO film. The demonstration of the 10nm atomically engineered HZO with a large piezoelectric response paves the way for extreme miniaturization of nano-mechanical resonators to mm-wave regime and for 5G applications. Besides, the low-temperature and truly conformal nature of ALD HZO process offers substantial advantages over conventional magnetron-sputtered / MOCVD films, including CMOS-compatibility and sidewall transducer integration. Finally, the capability to engineer the material properties by varying the dopant layering to enhance ferroelectricity and piezoelectricity or by applying DC bias to tune them, increases the potential of the proposed piezoelectric HZO many-fold.

Acknowledgment

This work was supported in part by NSF grants ECCS 1610387 and ECCS 1752206. The authors would like to thank Nanoscale Research Facility staff at the University of Florida and Nicholas Rudawski for help with TEM.

References

[1] Ramezani, M., et. al. IEEE IEDM, *2017* (pp. 40-41).
[2] Bahr, B., et al. IEEE ISSCC, *2018* (pp. 348-350).
[3] Yarar, E., et al. AIP Advances 6.7 (2016): 075115.
[4] Müller, J., et al. *ECS J. Solid State Sci. & Techno.* 4.5 (2015): N30-N35.
[5] Lomenzo, P. et al., APL 105, 072906 (2014).
[6] Polakowski, P., Müller, J., APL 106, 232905 (2015).
[7] Ghatge, M., et. al. IEEE Transducers, *2017* (pp. 746-749).
[8] Hyuk Park, Min, et al. APL 104, 072901 (2014).

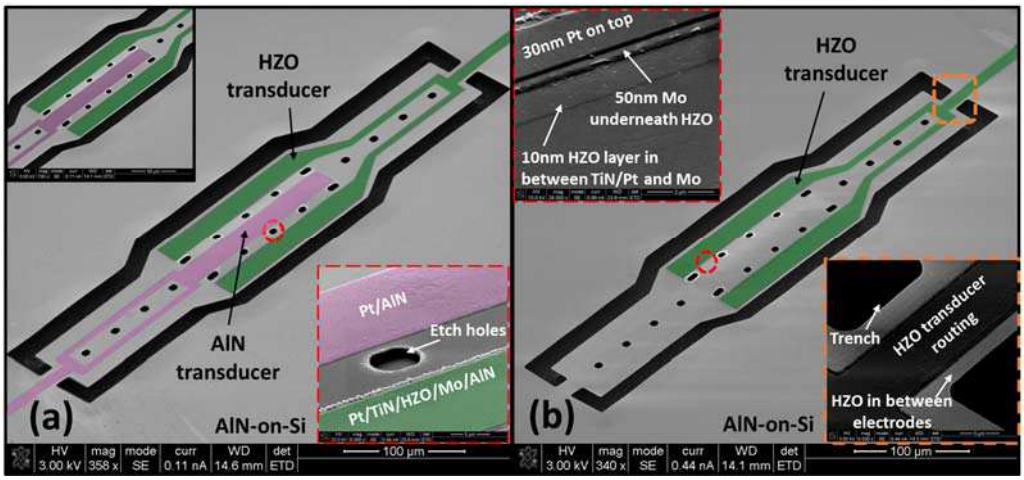

Fig. 1. (a) SEM image of two-port resonator. Port-1 (highlighted in pink) is an AlN transducer while port-2 (highlighted in green) is 10nm HZO transducer. (inset-top) shows the zoomed-in image of the transducer region. (inset-bottom) shows the close-up of the etch holes. (b) SEM image of 1-port HZO transduced resonator. (inset-top) highlights the HZO transducer stack. 10nm HZO is sandwiched between 30nm/10nm Pt/TiN on the top and 50nm Mo underneath. The wider HZO region helps avoid plausible shorting between the electrodes thus enabling viable transduction. (inset-bottom) shows routing of HZO transducer following same strategy as (inset-top) to avoid shorting of electrodes.

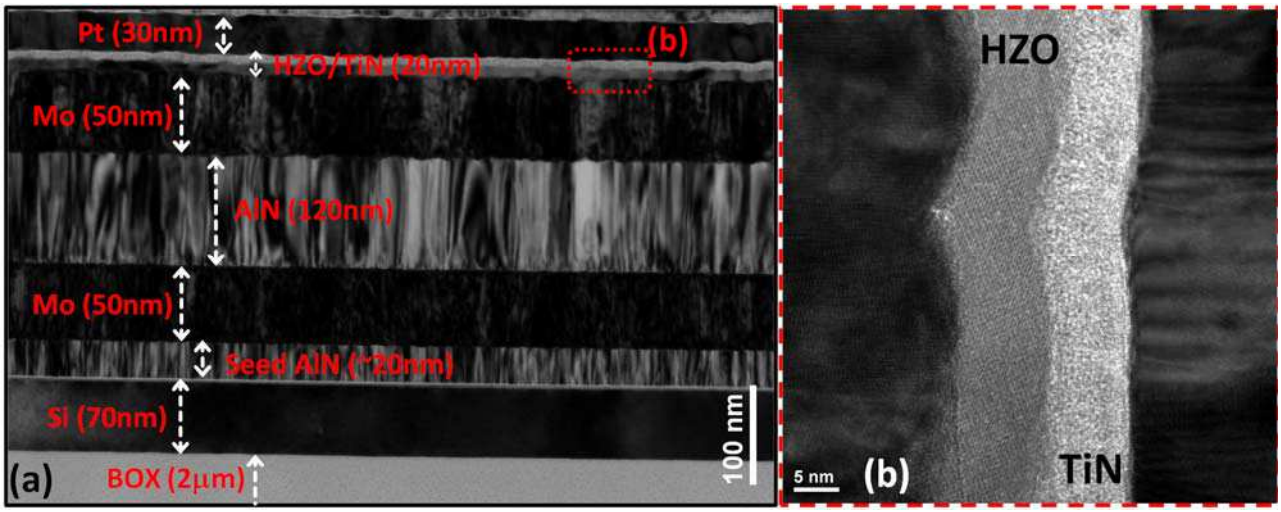

Fig. 2. (a) HR-XTEM image verifying the individual thicknesses of the materials in the stack. The c-axis oriented ~120nm AlN is evident on top of 50nm Mo. (b) Zoomed-in view of the 10nm/10nm HZO/TiN layers. The crystal diffraction patters are evident in HZO indicating the crystalline form of HZO. The conformal ALD deposition of HZO is unaffected by the topography of the bottom surface.

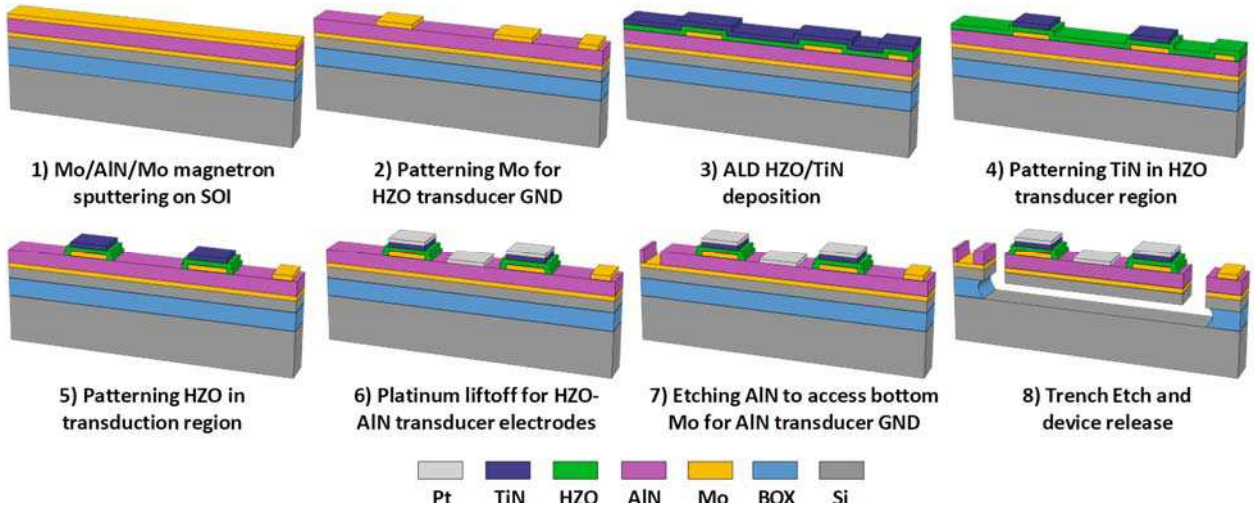

Fig. 3. The fabrication process flow for HZO/AlN dual-transduced 2-port resonator on 70nm Si. 120nm AlN is magnetron sputtered in between 50nm Mo layers. Top Mo acts as GND for HZO transducer while bottom Mo serves as GND for AlN transducer.

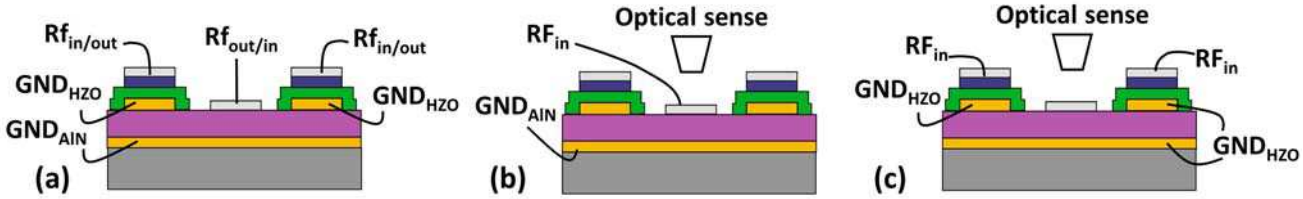

Fig. 4. (a) 2-port measurement set-up with AlN-drive and HZO-sense or vice versa. (b) AlN-drive and optical sense for the vibration using DHM. (c) HZO-drive and optical sense for vibrations using DHM.

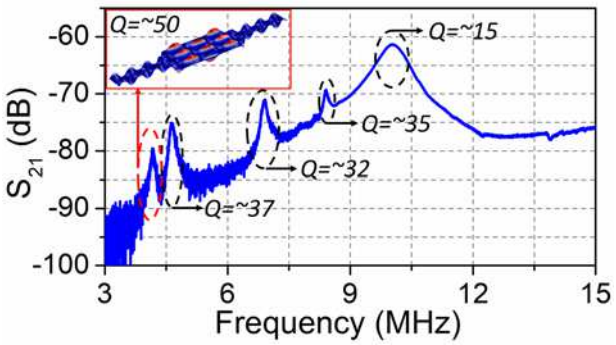

Fig. 5. Measured 2-port frequency response from 3MHz-15MHz operating for resonator design shown in Fig. 1(a). The maximum Q of ~50 (in air) at ~4.1MHz is observed. The resonator is actuated and sensed using the drive/sense mechanism shown in Fig. 4(a).

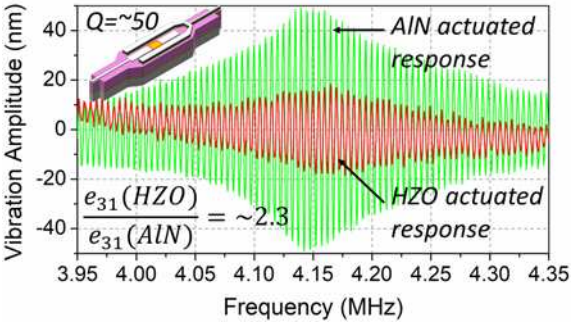

Fig. 6. Out-of-plane vibration amplitude for mode at ~4.1MHz actuated using driving mechanisms (Fig. 4(b) and Fig. 4(c)) with V_{drive}=2V. The AlN-actuated vibration amplitude (green) is ~50nm while HZO-actuated amplitude is ~20nm. The vibration amplitude comparison indicate $e_{31,HZO} \approx 2.3 e_{31,AlN}$.

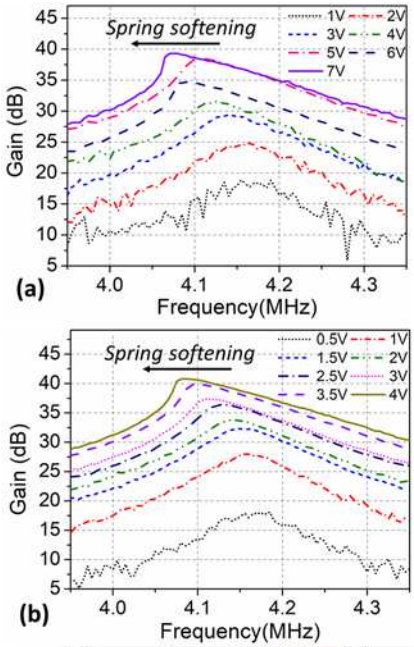

Fig. 7. (a) Short-span frequency response with power handling for ~4.1MHz mode with driving scheme shown in Fig. 4(c) (b) Short-span frequency response with power handling for the same mode with driving scheme shown in Fig. 4(b). AlN transducer is driven to non-linearity much sooner compared to HZO due to large vibration amplitude for the same bias voltage as shown in Fig. 6. The gain for the respective mode is derived using the vibration amplitudes captured using DHM at different input biases.

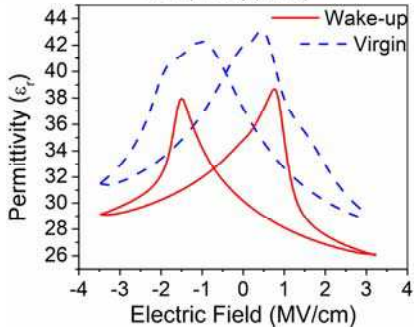

Fig. 10. Permittivity vs voltage for HZO reveals the signature dual CV peak for ferroelectric materials. The peak is more pronounced after wake-up. The tunable high-k dielectric nature of HZO is evident.

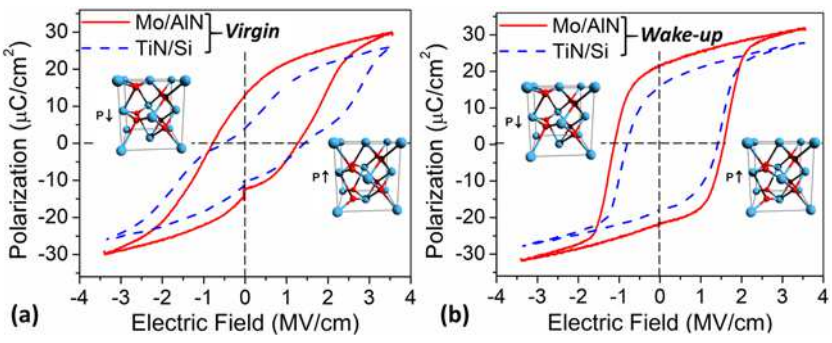

Fig. 8. Hysteresis curves for 10nm HZO on TiN/Si (dashed) and Mo/AlN (solid) in the virgin state (after RTA) (a) and after wake-up (b) achieved by 10k cycles of bipolar square wave at 1kHz. The remanent polarization (P_r) for HZO/Mo/AlN is higher than that of HZO/TiN/Si used typically signifying higher ferroelectricity.

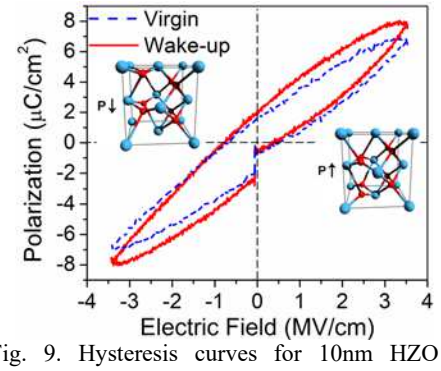

Fig. 9. Hysteresis curves for 10nm HZO transducer. The reduced P_r compared to Fig. 8(b) is attributed to smaller ferroelectric capacitor area and HF attacking HZO during release.